ADVANCED OPTICAL MATERIALS
www.advopticalmat.de

Spin-Selective Full and Subtle Light Intensity Manipulation with Diatomic Metasurfaces

Jiaqi Cheng, Zhancheng Li, Duk-Yong Choi, Shiwang Yu, Wenwei Liu, Haoyu Wang, Yuebian Zhang, Hua Cheng,* Jianguo Tian, and Shuqi Chen**

Metasurfaces are considered to be ideal candidates for precise and continuous manipulation of optical wave intensity at nanoscale pixels, which is the main basis of display and imaging devices. Malus's law has been widely used as the basic design principle for the realization of linearly polarized optical wave intensity manipulation. However, there is no such straightforward and concise law like Malus's law that can be used to design metasurfaces for full and subtle intensity manipulation of circularly polarized optical waves. Here, a new design strategy based on the collective interference effect in diatomic metasurfaces is presented to fill this gap, which can create a simple and complete mapping from a single structural variable to the reflection intensity of circularly polarized waves. The full and subtle intensity manipulation of circularly polarized optical waves can be conveniently realized by changing one structural parameter in the diatomic metasurface. Spin-selective high-level grayscale images are numerically and experimentally implemented based on the proposed diatomic metasurfaces. The proposed grayscale imaging scheme with subwavelength spatial resolution and high gray level is promising for advanced display and information encryption applications.

1. Introduction

Optical images are gradually demanded to have high spatial resolution, data density, and stability, aiming to meet the compelling requirements in many modern photonics applications. Metasurfaces have emerged as a powerful platform for fulfilling the above requirements of optical images due to their great precision and exceptional capabilities on light intensity manipulation at the subwavelength scale. It has been proven that metasurfaces can arbitrarily and independently manipulate light intensity by varying the sizes and orientation angles of nanostructures in every unit cell, enabling high-quality optical images.[1,2] Numerous intriguing designs of metasurfaces with high performance on light intensity manipulation have been widely used for the realization of image display,[3–9] image steganography,[10,11] information storage,[12–15] information encryption,[16–18] security and anti-counterfeiting,[19–21] and so forth. Recent progress in intensity-modulated metasurfaces has realized full and arbitrary intensity manipulation of linearly polarized waves, which can be easily manipulated by orientating the angle of nanostructures based on Malus's law, leading to a wide range of applications in high-resolution grayscale images and vivid color image display.[9,10] However, the realization of full and arbitrary intensity manipulation of circularly polarized waves is much more complicated since there is no such straightforward and concise law like Malus's law that can be used to guide the design of metasurfaces.

Recently, metasurfaces with chiral optical responses have been used for spin-selective transmission [22–28] and complex-amplitude modulation,[29–31] which are easy access to realize intensity manipulation of circularly polarized waves and spin-selective grayscale images. For example, two V-shaped nanostructures possessing different intensity manipulation results for left-handed circularly polarized (LCP) and right-handed circularly polarized (RCP) optical waves can be used to display spin-selective grayscale imaging.[6] However, an additional linear polarizer is required as an analyzer to decode grayscale image information in this strategy, limiting its practical applications. Another direct approach is utilizing dielectric polyatomic metasurfaces, in which the polarization-dependent constructive and destructive interference effects can be easily modulated by precisely controlling the geometric phase and the propagation phase simultaneously.[32] Such designs require fastidious adjustment of both the sizes and orientation angles of every nanostructure, which increases the design complexity. The period of unit cells in such designs is comparable to or larger than the operation wavelengths, which may cause unwanted high-order diffraction under oblique illuminations. The chiral mirror was

J. Cheng, Z. Li, S. Yu, W. Liu, H. Wang, Y. Zhang, H. Cheng, J. Tian, S. Chen
The Key Laboratory of Weak Light Nonlinear Photonics,
Ministry of Education, Smart Sensing Interdisciplinary Science Center,
Renewable Energy Conversion and Storage Center, School of Physics
and TEDA Institute of Applied Physics
Nankai University
Tianjin 300071, China
E-mail: zcli@nankai.edu.cn; hcheng@nankai.edu.cn; schen@nankai.edu.cn

D.-Y. Choi
Department of Quantum Science and Technology
Research School of Physics
Australian National University
Canberra, ACT 2601, Australia

S. Chen
The Collaborative Innovation Center of Extreme Optics
Shanxi University
Taiyuan 030006, China

DOI: 10.1002/adom.202202329

recently proposed to realize spin-selective reflected optical wave manipulation.[33] However, the accuracy of intensity manipulation is seriously limited as the variation of intensities with structural parameters is dramatic, and only low-level grayscale imaging can be realized. A straightforward and concise design for full and subtle intensity manipulation of circularly polarized optical waves with metasurfaces is highly desirable.

Here, we propose a new design strategy based on the collective interference effect in diatomic metasurfaces consisting of two umbrella-shaped nanostructures to realize spin-selective full and subtle intensity manipulation of optical waves. We numerically and experimentally prove that the reflection intensity of one circularly polarized wave can be fully and subtly manipulated with high efficiency by simply changing one structural variable, while that of the other circularly polarized wave remains unchanged. The potential application of our design in high-resolution and high-level grayscale imaging has also been experimentally demonstrated, which shows great practical importance to promote the improvement of spin-selective grayscale imaging and optical encryption.

2. Results and Discussion

Figure 1 illustrates the structural configuration of the proposed diatomic metasurface and the spin-selective light intensity manipulation. The diatomic metasurface is a metal-insulator-metal design consisting of two umbrella-shaped structures in every unit cell. The reflection intensity of RCP waves can continuously decrease with increasing structural variable β_2. Consequently, precise and continuous intensity manipulation of RCP waves can be realized. The thicknesses of the aluminum umbrella-shaped structures, the silicon dioxide spacer layer, and the ground aluminum layer are $h_1 = 50$ nm, $h_2 = 150$ nm, and $h_3 = 100$ nm, respectively. The periods in both the x and y directions are $P_x = P_y = 650$ nm. The structural parameters of the two umbrella-shaped structures are: $r_1 = 110$ nm, $r_2 = 170$ nm, $w = 60$ nm, $L = 340$ nm, and $G = 240$ nm, where r_1 and r_2 are the internal and external radii, w and L are the width and length of the umbrella handle (L is twice the length of r_2.), and G is the distance between the two umbrella-shaped structures. We define the two umbrella-shaped structures as structure 1 (S1) and structure 2 (S2), as presented in Figure 1. The angles α_1 and α_2 correspond to the length of the clockwise arcs, and the angles β_1 and β_2 correspond to the length of the anticlockwise arcs. The angles α_1, α_2, and β_1 are fixed at 40°, while the angle β_2 is defined as the structural variable to manipulate the reflection intensity of RCP waves that is modulated from 40° to 130°. The angles α_1 and α_2 can also be set to other values as long as they are equal since the spin-selective light intensity manipulation is mainly derived from the difference between the angles β_1 and β_2. The changes in angles α_1 and α_2 can slightly affect the reflection intensities of LCP and RCP waves. Here, we optimized and set the angles α_1, α_2, and β_1 to 40° to obtain the best performance of spin-selective light intensity manipulation.

To reveal the relationship between the structural variable β_2 and the reflection intensity, we analyzed the optical characteristics of the two designed diatomic metasurfaces with $\beta_2 =$ 40° and 130°. Figure 2a,b shows the simulated squared moduli $r_{ij} = |R_{ij}|^2$ of two diatomic metasurfaces, where subscripts "i" and "j" denote the polarization states of the reflected and incident waves. There is no chiral response for the diatomic metasurface with $\beta_2 = 40°$ as it has a C_{2z} rotational symmetry (shown in **Figure 2**a), which can be regarded as a broadband and efficient

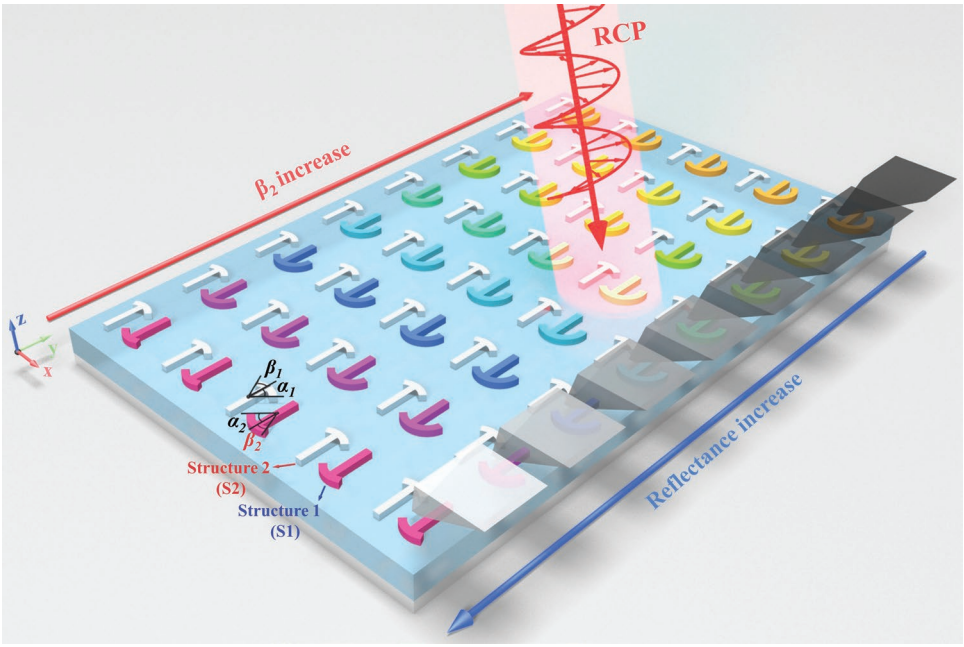

Figure 1. Illustration of the designed diatomic metasurface and its functional demonstration for full and subtle intensity manipulation of RCP waves. The diatomic metasurface consists of two umbrella-shaped structures in every unit cell, which are abbreviated as S1 and S2. Two structural variables of angles β_1 and β_2 correspond to the length of the anticlockwise arcs in S1 and S2, related to the manipulation of RCP waves. The reflection intensity of RCP waves continuously decreases as β_2 increases. The single structural variable is modulated to induce a variety of reflection intensities of RCP waves.

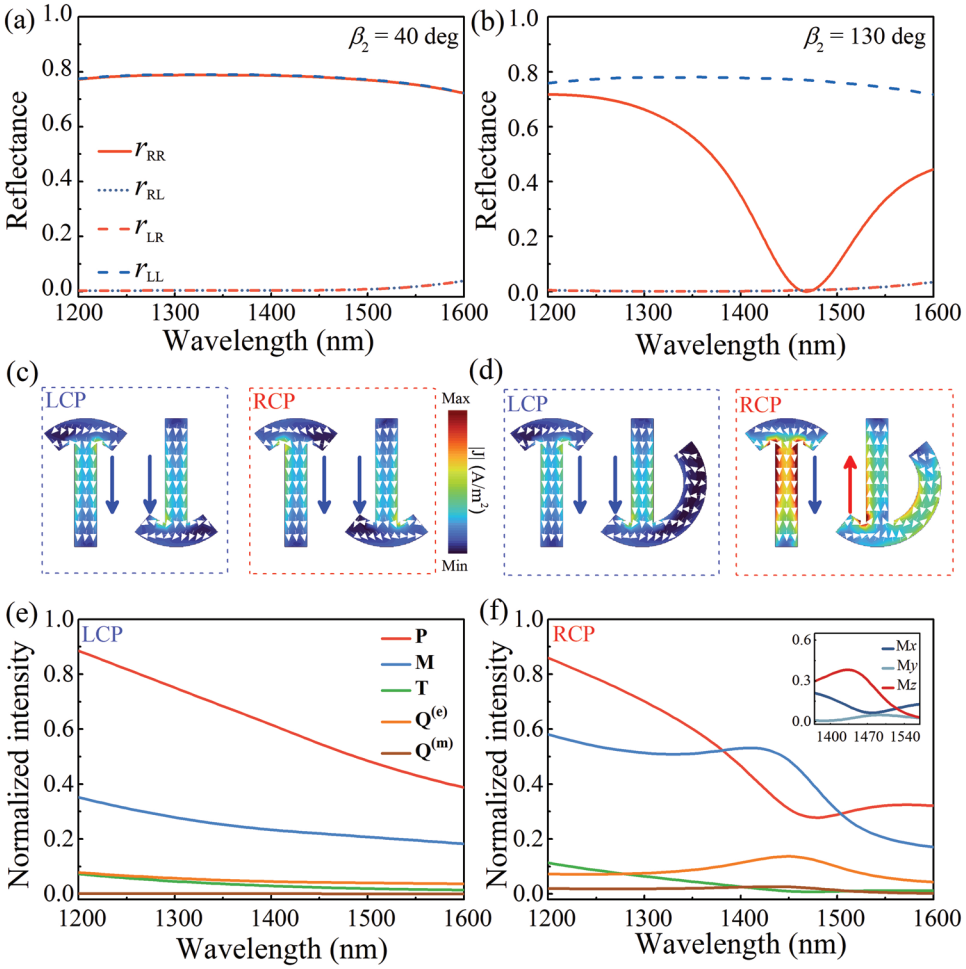

Figure 2. Simulated reflection spectra of two designed diatomic metasurfaces and analysis on the physical mechanisms of the spin-selective reflection. Simulated squared moduli $r_{ij} = |R_{ij}|^2$ for the proposed diatomic metasurfaces with a) $\beta_2 = 40°$ and b) $\beta_2 = 130°$. Simulated current flow (white arrow) and current density on the middle section of the nanostructures in one unit cell at 1470 nm under LCP and RCP illuminations: c) $\beta_2 = 40°$ and d) $\beta_2 = 130°$. Multipolar decomposition of scattering power spectra of diatomic metasurface with $\beta_2 = 130°$ under e) LCP and f) RCP illuminations. The inset in (f) shows the scattering intensities of the components of the magnetic dipole under RCP illumination.

circular polarization-preserving mirror in the wavelength range of 1200 to 1600 nm. The spin-flipped reflection intensities r_{RR} and r_{LL} are both high and remain at an approximately constant value of 0.78, while the spin-preserved reflection intensities r_{LR} and r_{RL} are both close to zero. In contrast, the diatomic metasurface with $\beta_2 = 130°$ breaks the structural rotation symmetry and has a significant chiral optical response, as shown in Figure 2b. It operates as a chiral mirror that can reflect LCP waves without polarization change while exhibiting a near-perfect extinction of RCP waves at the operation wavelength. The reflection intensity r_{LL} is greater than 0.78 at 1470 nm while r_{RR} is lower than 0.001. The spin-preserved reflection intensities r_{LR} and r_{RL} are both lower than 0.005. These results indicate that the reflection intensity of RCP waves can be manipulated by changing β_2 from 40° to 130°, while the reflection intensity of LCP waves can remain almost constant. To further reveal the underlying physics, we simulated the distributions of the current flows in the cross-section of the two diatomic metasurfaces at 1470 nm under LCP and RCP illuminations, as shown in Figure 2c,d. The distributions of current flows for $\beta_2 = 40°$ are almost the same under LCP and RCP illuminations, which is related to achiral resonance. The currents on the handles of S1 and S2 can be treated as a pair of parallel electric dipoles to form a symmetric resonant mode under both LCP and RCP illuminations, as represented by the blue arrows in Figure 2c. The resonant mode of the diatomic metasurface can be apparently changed by adjusting β_2 from 40° to 130°, as shown in Figure 2d. The resonant modes of the diatomic metasurface for $\beta_2 = 40°$ and 130° are similar to each other under LCP illumination. The length of the anticlockwise arcs does not affect the resonant mode under LCP illumination. In contrast, the resonant modes of the diatomic metasurface for $\beta_2 = 40°$ and 130° are notably different from each other under RCP illumination. The currents on the handles of S1 and S2 represented by the red and blue arrows in Figure 2d can be equivalent to a pair of anti-parallel electric dipoles to form an anti-symmetric resonant mode, which results in a magnetic dipole along the *z*-axis and the suppression of the far-field radiation. To make a quantitative validation, we decomposed the scattering intensity of the diatomic metasurface into multipolar modes (electric dipole

(**P**), magnetic dipole (**M**), toroidal dipole (**T**), electric quadrupole ($\mathbf{Q}^{(e)}$), and magnetic quadrupole ($\mathbf{Q}^{(m)}$) modes) based on the electromagnetic multipole expansion method. The scattering intensity of each electromagnetic multipolar mode can be expressed as[34–36]

$$I = \frac{2\omega^4}{3c^3}|\mathbf{P}|^2 + \frac{2\omega^4}{3c^3}|\mathbf{M}|^2 + \frac{2\omega^6}{3c^5}|\mathbf{T}|^2 + \frac{\omega^6}{5c^5}\Sigma|Q^{(e)}_{\alpha\beta}|^2 + \frac{\omega^6}{40c^5}\Sigma|Q^{(m)}_{\alpha\beta}|^2 + \cdots \quad (1)$$

where α and β represent x, y, and z. Figure 2e,f illustrates the calculated results of the scattering intensity spectra of the diatomic metasurface with $\beta_2 = 130°$ under LCP and RCP illuminations, respectively. The electric dipole P in the diatomic metasurface makes a dominant contribution to the far-field radiation, and the suppression of the electric dipole P corresponds to the decrease in reflection intensity. The inset in Figure 2f validates the enhancement of the z-component of the magnetic dipole M under RCP illumination. These results are in good agreement with the qualitative analysis based on Figure 2c,d. The symmetric and anti-symmetric resonant modes are correlated to the constructive and destructive interference of the far-field radiation from the electric dipoles in S1 and S2. The variation of spin-selective reflection intensity is directly associated with the spin-selective resonant mode modulation by adjusting β_2.

We further justify the capacity of the designed diatomic metasurfaces for full and subtle spin-selective light intensity manipulation by revealing the relationship between the collective interference effect and the angle β_2. The y-component distributions of the currents on the anticlockwise arcs and the handles of S1 and S2 under RCP illumination are related to a pair of electric dipoles oscillating along the y-direction, which can be expressed as:

$$P_y = \frac{1}{i\omega}\int J_y d^3r \quad (2)$$

where $J_y(\mathbf{r}) = i\omega\varepsilon_0(\tilde{\varepsilon}_r - 1)E_y(\mathbf{r})$ and ω, ε_0, $\tilde{\varepsilon}_r$, and $E_y(\mathbf{r})$ are the angular frequency of light field, the free-space permittivity, the complex-valued dielectric constant, and the y-component of the electric field in the space position **r**. We assume that the electric dipoles in S1 and S2 are P_1 and P_2. Then, we defined the ratio of the amplitude of P_1 and P_2 as $\gamma = |P_2/P_1|$, and the phase difference between the two electric dipoles as $\Delta\varphi = \varphi_2 - \varphi_1$ (φ_1 and φ_2 are the phases of P_1 and P_2). The far-field radiation related to the superimposition of P_1 and P_2 at a fixed wavelength can then be expressed as:[36,37]

$$E_s \propto 1 + \gamma e^{i\Delta\varphi} \quad (3)$$

Obviously, destructive and constructive interference occurs when $\Delta\varphi = n\pi$ and $\Delta\varphi = 2n\pi$ (n is an integer) while $\gamma = 1$. We calculated the complex amplitudes P_y in S1, S2, and S1 + S2 of the diatomic metasurface with $\beta_2 = 130°$ under both LCP and RCP illuminations, as plotted in **Figure 3**a,b. For LCP illumination, $\gamma = 1$ and $\Delta\varphi$ is close to 0, representing the constructive interference between P_1 and P_2. In contrast, for RCP illumination, $\gamma = 1$ at the operation wavelength of 1470 nm while $\Delta\varphi$ is close to π, indicating destructive interference between P_1 and P_2. These results have also been qualitatively validated based on the

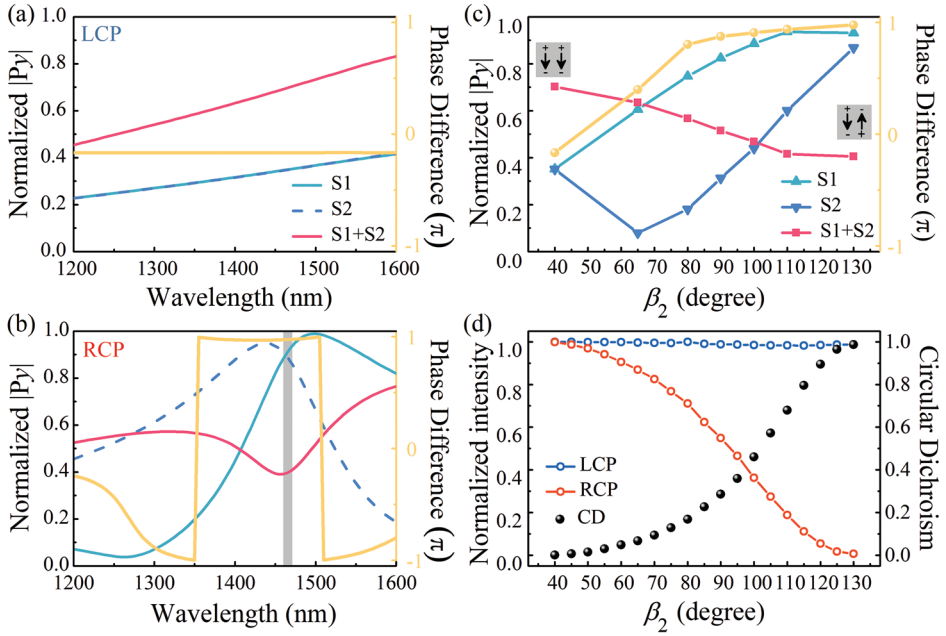

Figure 3. Realizing the spin-selective full and subtle intensity manipulation of RCP waves based on the optical collective interference effect. The amplitude and phase difference of the y-component of the electric dipoles (P_y) within S1 and S2 with $\beta_2 = 130°$ under a) LCP and b) RCP illuminations. c) The variation of amplitude and phase difference of P_y within S1 and S2 at 1470 nm under RCP illumination as a function of the structural variable β_2. The resonant mode of electric dipoles in S1 and S2 converts from symmetric mode to anti-symmetric mode with the increase of β_2. d) Simulated reflection intensities and circular dichroism (defined as $\Delta r = (r_{LCP} - r_{RCP})/(r_{LCP} + r_{RCP})$) at 1470 nm with the variation of the structural variable β_2. The reflection intensities are normalized with the maximum value.

simulated distributions of current flows within S1 and S2 (Figure S1, Supporting Information). The effect of collective interference can be tuned by adjusting β_2. The increase of β_2 will induce extra currents in the anticlockwise arc of S2. The oscillation of the currents in S2 will be delayed, resulting in an extra phase delay (named Aharonov–Anandan (AA) geometric phase[38]) of the reflection waves. The resonance of S2 and its interaction with the resonance of S1 will therefore be changed. We further simulated the variation of the complex amplitudes P_y in S1, S2, and S1 + S2 of the diatomic metasurfaces with different β_2 at 1470 nm under RCP illumination in Figure 3c. The phase difference ($\Delta\varphi$) of P_1 and P_2 increases with increasing β_2 after the structural rotation symmetry is broken. As a result, P_1 and P_2 gradually convert from in-phase oscillation to out-of-phase oscillation with increasing β_2. This conversion process has also been validated by simulating the distributions of current flows within S1 and S2 (Figure S2, Supporting Information). The total electric dipole P_y in S1 and S2 monotonously decreases with increasing β_2 at 1470 nm, resulting in a monotonously decreasing reflection intensity with increasing β_2 at 1470 nm under RCP illumination. We simulated the variation of reflection intensities of the diatomic metasurfaces with the increase of β_2 under both LCP and RCP illuminations at 1470 nm and calculated the corresponding circular dichroism (defined as $\Delta r = (r_{LCP} - r_{RCP})/(r_{LCP} + r_{RCP})$) spectra, as shown in Figure 3d. The reflection intensity of RCP waves can be continuously and flexibly manipulated as β_2 varies from 40° to 130°, while the reflection intensity of LCP waves remains constant, resulting in the spin-selective full and subtle intensity manipulation of optical waves. Note that the spin-preserved reflection intensities r_{LR} and r_{RL} are close to 0 and remain almost unchanged as β_2 varies, which means that the spin-flipped reflection intensity r_{RR} is continuously manipulated as β_2 varies from 40° to 130°. The relationship between the reflection intensity of RCP waves and the angle β_2 is similar to that between the transmission intensity of linearly polarized illumination and the orientation angle of the polarizer in Malus's law. Moreover, full and subtle intensity manipulation of LCP waves can be further realized by swapping the positions of S1 and S2 to form an enantiomorph of the designed diatomic metasurface and changing angle α_2 (or α_1) from 40° to 130°, while the reflection intensity of RCP waves remains constant. Note that adjusting the distance G between the two structures within a certain range does not affect the spin-selective light intensity manipulation but only causes a slight shift of the operation wavelength. With the above deep insight into the physical mechanism, we have successfully demonstrated the simple and complete mapping from the structural variable β_2 to the intensities of reflected RCP waves. Therefore, arbitrary reflection intensity manipulation of RCP waves can be realized by simply choosing the appropriate value of angle β_2.

The advantages of the proposed diatomic metasurface on spin-selective full and subtle intensity manipulation of optical waves have also been experimentally validated. We fabricated seven periodic diatomic metasurfaces with β_2 = 40°, 65°, 80°, 90°, 100°, 110°, and 130°. The top-view scanning electron microscope (SEM) images of three of them (β_2 = 40°, 90°, and 130°) are shown in **Figure 4**a. We measured the reflection spectra of the fabricated metasurfaces based on our custom-built optical setting (details in Experimental Section). Figure 4b,c shows the simulated and measured reflection spectra of the diatomic metasurfaces with β_2 = 40°, 80°, 90°, 100°, and 130° under LCP and

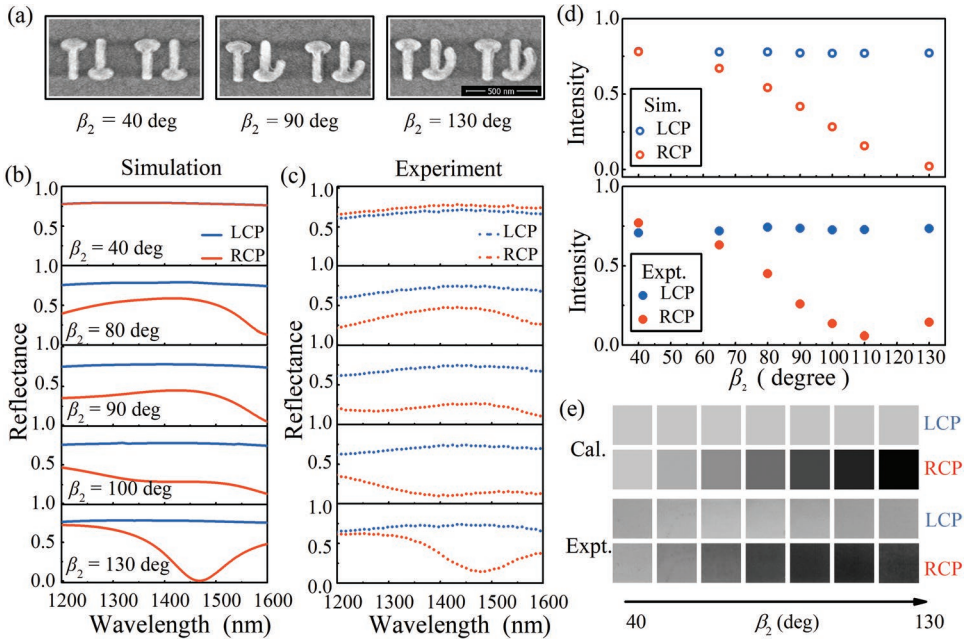

Figure 4. Experimental validation of spin-selective light intensity manipulation based on the proposed diatomic metasurfaces. a) SEM images of the designed diatomic metasurfaces with β_2 = 40°, 90°, and 130°. The scale bar is 500 nm. b) Simulated and c) measured reflection spectra of the designed diatomic metasurfaces with different β_2 values under LCP and RCP illuminations. d) The simulated and measured reflection intensities of the designed diatomic metasurfaces with different β_2 values at 1480 nm. e) Calculated and measured grayscale images of the periodic diatomic metasurfaces with different β_2 values at 1480 nm under LCP and RCP illuminations.

RCP illuminations. The measured results are in good agreement with the simulated results. The operation wavelength is red-shifted to 1480 nm in the experimental measurement. The difference between the simulated and measured results can be attributed to the sample fabrication error (A detailed discussion can be found in Figure S3, Supporting Information). To intuitively display the performance of the designed diatomic metasurface on spin-selective light intensity manipulation, we give the simulated and measured reflection intensities of the seven designed diatomic metasurfaces at 1480 nm under both LCP and RCP illuminations in Figure 4d. The simulated and measured intensities can maintain about 0.78 and 0.72 under LCP illumination respectively. They change from 0.78 to 0.02 and 0.77 to 0.05 under RCP illumination. The modulation of the reflection intensity indicates that the designed diatomic metasurface can be used to realize reflection intensity manipulation at 1480 nm under RCP illumination, while the reflection intensity of LCP waves can remain almost unchanged. We also numerically calculated and experimentally captured the grayscale images of the seven designed diatomic metasurfaces, as presented in Figure 4e. These results indicate that spin-selective high-level grayscale imaging can be achieved based on the designed diatomic metasurfaces.

To show the performance of the high-level grayscale images for the presented diatomic metasurfaces, we designed, fabricated, and measured several aperiodic diatomic metasurfaces containing different grayscale image information. As shown in **Figure** 5, we designed a two-level and a 19-level grayscale image of a sketch tiger, and a 15-level grayscale image of a jigsaw puzzle. All three designed samples are composed of 300 × 300 pixels, and every pixel represents a unit cell with a given value of β_2 to record the grayscale information. The designed samples were measured by using our custom-built optical setting and adding a narrow-band interference filter with a center wavelength of 1480 nm (details in Experimental Section). As shown in Figure 5a, the designed grayscale images of a sketch tiger can be observed only under the illumination of RCP waves, and the 19-level grayscale image shows more details than the two-level image. As an example, the tiger tongues are enlarged to show the wealthier grayscale of the 19-level grayscale image. The edges of the measured grayscale images are not very clear. This is attributed to the imaging aberration of the measurement system. The results in Figure 5a prove that the proposed diatomic metasurface with the capacity of spin-selective full and subtle reflection intensity manipulation can be used to realize high-level and high-resolution grayscale images. The calculated and measured 15-level grayscale images of a jigsaw puzzle can more clearly show the power of the designed diatomic metasurface for continuous and subtle reflection intensity manipulation under RCP illumination, as shown in Figure 5b. The difference of the grayscale in different areas can be easily observed by large pixels. To perform a quantitative analysis, we extracted and plotted the intensity data along the solid and dashed lines (marked in Figure 5b) from A to B and C to D in Figure 5c,d, respectively. The calculated and measured results are in reasonable agreement with each other, which further proves the capacity of the designed metasurfaces for the realization of high-level grayscale images.

3. Conclusion

In conclusion, we presented a new design strategy for diatomic metasurfaces based on the resonance collective interference

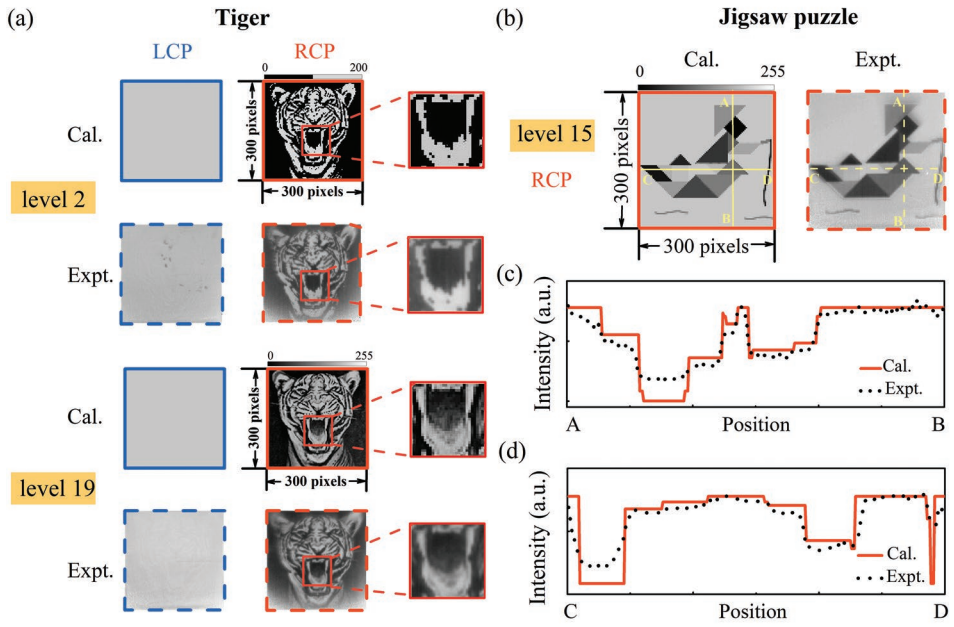

Figure 5. Realization of spin-selective high-level grayscale imaging based on the proposed diatomic metasurfaces. a) Calculated and measured grayscale tiger images with different gray levels at 1480 nm under LCP and RCP illuminations (highlighted by blue and red boxes). The magnifying parts show the details of the tiger tongue. b) Calculated and measured jigsaw puzzle image with 15-gray-level gray at 1480 nm under RCP illumination. c) Extracted intensity data along the solid line and dashed line from A to B marked on the calculated and measured images in (b). d) Extracted intensity data along the solid line and dashed line from C to D marked on the calculated and measured images in (b).

effect for the realization of spin-selective full and subtle light intensity manipulation, which creates a simple and complete mapping from a single structural variable to the reflection intensity of circularly polarized waves. We designed diatomic metasurfaces consisting of two umbrella-shaped structures and validated that the resonances in the two umbrella-shaped structures can gradually convert from in-phase oscillation to out-of-phase oscillation with increasing structural variable β_2, resulting in full and subtle light intensity manipulation. Both the simulated and measured results proved that the proposed diatomic metasurfaces exhibit outstanding flexibility to modulate the reflection intensity of RCP waves. The experimental results validate that, with the increase of β_2, the reflection intensity at the operation wavelength fluctuates around 0.72 under LCP illumination, while it changes from 0.77 to 0.05 under RCP illumination. We further experimentally demonstrated the outstanding capacity of the designed diatomic metasurface for the realization of high-level and high-resolution grayscale images. Our work provides a concise method to fully and subtly manipulate the reflection intensity of circularly polarized waves, which will act as a versatile platform for advanced image display, high-density optical data storage, and information encryption.

4. Experimental Section

Sample Fabrication: The proposed diatomic metasurfaces were fabricated by electron-beam lithography (EBL) and aluminum lift-off processes. A 100 nm thick aluminum film was initially deposited onto a microscope slide glass by using an electron-beam evaporator (Temescal BJD-2000). A 150 nm thick SiO_2 layer was subsequently deposited onto the sample by using plasma-enhanced chemical vapor deposition. After that, a 200 nm thick positive electron-beam resist of ZEP520A was spin-coated, and then the structure pattern was exposed using an EBL system (RAITH 150) at 30 keV. After the exposure, the sample was developed in n-amyl acetate for 60 s, rinsed with isopropyl alcohol, and then blown dry using nitrogen. A 50 nm thick aluminum film was subsequently deposited by using an electron-beam evaporator (Temescal BJD-2000). After the resist was removed by means of a ZEP remover (ZDMAC), the diatomic metasurfaces were created.

Numerical Simulations: Numerical simulations were conducted using finite differential time domain methods. The optical constants of aluminum were taken from experimental data,[39] and the refractive index of SiO_2 was taken as 1.5. The periodic boundary conditions were set in the *x* and *y* directions to represent a periodical structure, and the waveguide port boundary was defined in the *z* direction for light incidence and reflectance. The excitation source was either a left-handed or right-handed circularly polarized plane wave.

Experimental Measurement: The experimental measurement of the proposed designed metasurfaces was based on custom-built optical settings (Figure S4, Supporting Information). A bromine tungsten lamp (Zolix, LSH-150) collimated by a fiber collimator was used as the light source for the measurement of the reflection spectrum. The collimated beam passed through a broadband polarizer (Thorlabs, LPNIR050-MP2), and an achromatic quarter-wave plate (B. Halle Nachfl, $\lambda/4$ super achromatic waveplates) to generate a circularly polarized beam. The circularly polarized beam then passed through a broadband unpolarized beam splitting prism (MFOPT, OQNP25.4N-NIR-3) and was focused on the sample with an objective (Sigma NIR plan apo 20×, NA = 0.45). The collected reflection beam passed through an achromatic quarter-wave plate (B. Halle Nachfl, $\lambda/4$ super achromatic waveplates) and a broadband polarizer (Thorlabs, LPNIR050-MP2). Then the beam passed through an aperture and a lens. The focused beam then passed through a broadband unpolarized beam splitting prism (MFOPT, OQNP25.4N-NIR-3) and was collected by an optical spectrum analyzer (Zolix, Omni-λ3007) via a fiber coupler and an InGaAs camera (HAMAMATSU InGaAs C10633). The reflection spectra data were acquired with the software of the optical spectrum analyzer. The silicon dioxide substrate and the underlying aluminum film were used as the reference for measuring the reflectance. The experimental setup for optical imaging was modified by adding a narrow-band interference filter (Thorlabs, FB1480-12) in front of the InGaAs camera. The output light from the objective and unpolarized beam-splitting prism was collected by the InGaAs camera, and the gray images were taken by the software of the camera.

Supporting Information

Supporting Information is available from the Wiley Online Library or from the author.

Acknowledgements

This work was supported by the National Key Research and Development Program of China (2021YFA1400601 and 2022YFA1404501), the National Natural Science Fund for Distinguished Young Scholars (11925403), the National Natural Science Foundation of China (12122406, 12192253, 11974193, 12274237, 12274239, and U22A20258), and the China Postdoctoral Science Foundation (2018M640224 and 2021M690084).

Conflict of Interest

The authors declare no conflict of interest.

Data Availability Statement

The data that support the findings of this study are available from the corresponding author upon reasonable request.

Keywords

collective interference, diatomic metasurfaces, grayscale imaging, spin-selective intensity manipulation

Received: October 3, 2022
Revised: November 24, 2022
Published online:

[1] A. M. Shaltout, N. Kinsey, J. Kim, R. Chandrasekar, J. C. Ndukaife, A. Boltasseva, V. M. Shalaev, *Proc. IEEE* **2016**, *104*, 2270.
[2] S. Yu, J. Cheng, Z. Li, W. Liu, H. Cheng, J. Tian, S. Chen, *ChemPhysMater* **2022**, *1*, 6.
[3] X. Zang, F. Dong, F. Yue, C. Zhang, L. Xu, Z. Song, M. Chen, P.-Y. Chen, G. S. Buller, Y. Zhu, S. Zhuang, W. Chu, S. Zhang, X. Chen, *Adv. Mater.* **2018**, *30*, 1707499.
[4] Q. Dai, L. Deng, J. Deng, J. Tao, Y. Yang, M. Chen, Z. Li, Z. Li, G. Zheng, *Opt. Express* **2019**, *27*, 27927.
[5] Z. Li, W. Liu, H. Cheng, D. Choi, S. Chen, J. Tian, *Adv. Opt. Mater.* **2019**, *7*, 1900260.
[6] Y. Chen, J. Gao, X. Yang, *Adv. Opt. Mater.* **2019**, *7*, 1801467.
[7] Y. Bao, Y. Yu, H. Xu, C. Guo, J. Li, S. Sun, Z.-K. Zhou, C.-W. Qiu, X.-H. Wang, *Light: Sci. Appl.* **2019**, *8*, 95.

[8] Z. Deng, M. Jin, X. Ye, S. Wang, T. Shi, J. Deng, N. Mao, Y. Cao, B. Guan, A. Alù, G. Li, X. Li, *Adv. Funct. Mater.* **2020**, *30*, 1910610.
[9] P. Huo, M. Song, W. Zhu, C. Zhang, L. Chen, H. J. Lezec, Y. Lu, A. Agrawal, T. Xu, *Optica* **2020**, *7*, 1171.
[10] F. Yue, C. Zhang, X.-F. Zang, D. Wen, B. D. Gerardot, S. Zhang, X. Chen, *Light: Sci. Appl.* **2018**, *7*, 17129.
[11] Z. Deng, Q. Tu, Y. Wang, Z. Wang, T. Shi, Z. Feng, X. Qiao, G. P. Wang, S. Xiao, X. Li, *Adv. Mater.* **2021**, *33*, 2103472.
[12] Y. Chen, X. Yang, J. Gao, *Light: Sci. Appl.* **2019**, *8*, 45.
[13] Q. Dai, Z. Guan, S. Chang, L. Deng, J. Tao, Z. Li, Z. Li, S. Yu, G. Zheng, S. Zhang, *Adv. Funct. Mater.* **2020**, *30*, 2003990.
[14] L. Deng, J. Deng, Z. Guan, J. Tao, Y. Chen, Y. Yang, D. Zhang, J. Tang, Z. Li, Z. Li, S. Yu, G. Zheng, H. Xu, C.-W. Qiu, S. Zhang, *Light: Sci. Appl.* **2020**, *9*, 101.
[15] Z. Li, C. Chen, Z. Guan, J. Tao, S. Chang, Q. Dai, Y. Xiao, Y. Cui, Y. Wang, S. Yu, G. Zheng, S. Zhang, *Laser Photonics Rev.* **2020**, *14*, 2000032.
[16] F. Walter, G. Li, C. Meier, S. Zhang, T. Zentgraf, *Nano Lett.* **2017**, *17*, 3171.
[17] Y. Tang, Y. Intaravanne, J. Deng, K. F. Li, X. Chen, G. Li, *Phys. Rev. Appl.* **2019**, *12*, 024028.
[18] P. Zheng, Q. Dai, Z. Li, Z. Ye, J. Xiong, H.-C. Liu, G. Zheng, S. Zhang, *Sci. Adv.* **2021**, *7*, abg0363.
[19] C. Zhang, D. Wen, F. Yue, Y. Intaravanne, W. Wang, X. Chen, *Phys. Rev. Appl.* **2018**, *10*, 034028.
[20] C. Zhang, F. Dong, Y. Intaravanne, X. Zang, L. Xu, Z. Song, G. Zheng, W. Wang, W. Chu, X. Chen, *Phys. Rev. Appl.* **2019**, *12*, 034028.
[21] J. Deng, L. Deng, Z. Guan, J. Tao, G. Li, Z. Li, Z. Li, S. Yu, G. Zheng, *Nano Lett.* **2020**, *20*, 1830.
[22] M. Kenney, S. Li, X. Zhang, X. Su, T.-T. Kim, D. Wang, D. Wu, C. Ouyang, J. Han, W. Zhang, H. Sun, S. Zhang, *Adv. Mater.* **2016**, *28*, 9567.
[23] F. Zhang, M. Pu, X. Li, P. Gao, X. Ma, J. Luo, H. Yu, X. Luo, *Adv. Funct. Mater.* **2017**, *27*, 1704295.
[24] D. Ma, Z. Li, Y. Zhang, W. Liu, H. Cheng, S. Chen, J. Tian, *Opt. Lett.* **2019**, *44*, 3805.
[25] X. Yin, M. Schäferling, B. Metzger, H. Giessen, *Nano Lett.* **2013**, *13*, 6238.
[26] Y. Zhang, Z. Li, W. Liu, Z. Li, H. Cheng, S. Chen, J. Tian, *Adv. Opt. Mater.* **2019**, *7*, 1801273.
[27] Y. Huang, T. Xiao, Z. Xie, J. Zheng, Y. Su, W. Chen, K. Liu, M. Tang, P. Müller-Buschbaum, L. Li, *Adv. Opt. Mater.* **2021**, *9*, 2001663.
[28] Y. Gou, H. F. Ma, Z. X. Wang, L. W. Wu, R. Y. Wu, T. J. Cui, *Opt. Express* **2022**, *30*, 12775.
[29] M. Liu, W. Zhu, P. Huo, L. Feng, M. Song, C. Zhang, L. Chen, H. J. Lezec, Y. Lu, A. Agrawal, T. Xu, *Light: Sci. Appl.* **2021**, *10*, 107.
[30] H. Wang, Y. Jing, Y. Li, L. Huang, M. Feng, Q. Yuan, H. Bai, J. Wang, J. Zhang, S. Qu, *Adv. Opt. Mater.* **2021**, *9*, 2100140.
[31] H. Wang, Y. Li, L. Huang, Y. Jing, Q. Yuan, J. Wang, J. Zhang, S. Qu, *Ann. Phys.* **2021**, *533*, 2000515.
[32] Q. Fan, M. Liu, C. Zhang, W. Zhu, Y. Wang, P. Lin, F. Yan, L. Chen, H. J. Lezec, Y. Lu, A. Agrawal, T. Xu, *Phys. Rev. Lett.* **2020**, *125*, 267402.
[33] Z. Li, W. Liu, H. Cheng, D. Choi, S. Chen, J. Tian, *Adv. Mater.* **2020**, *32*, 1907983.
[34] V. Savinov, V. A. Fedotov, N. I. Zheludev, *Phys. Rev. B* **2014**, *89*, 205112.
[35] N. Papasimakis, V. A. Fedotov, V. Savinov, T. A. Raybould, N. I. Zheludev, *Nat. Mater.* **2016**, *15*, 263.
[36] P. C. Wu, C. Y. Liao, V. Savinov, T. L. Chung, W. T. Chen, Y.-W. Huang, P. R. Wu, Y.-H. Chen, A.-Q. Liu, N. I. Zheludev, D. P. Tsai, *ACS Nano* **2018**, *12*, 1920.
[37] N. Li, Y. Lai, S. H. Lam, H. Bai, L. Shao, J. Wang, *Adv. Opt. Mater.* **2021**, *9*, 2001081.
[38] R. Ji, X. Xie, X. Guo, Y. Zhao, C. Jin, K. Song, S. Wang, J. Yin, Y. Liu, C. Jiang, C. Yang, X. Zhao, W. Lu, *ACS Photonics* **2021**, *8*, 1847.
[39] M. R. Querry, Optical Constants, Contractor report, US Army Chemical Research, Development, and Engineering Center (CRDEC), Aberdeen, Proving Ground, MD, USA **1985**.